Characterization of potassium carbonate salt hydrate for thermochemical energy storage in buildings

Energy & Buildings 196 (2019) 178–193

Contents lists available at ScienceDirect

Energy & Buildings

journal homepage: www.elsevier.com/locate/enbuild

Characterization of potassium carbonate salt hydrate for thermochemical energy storage in buildings

M. Gaeini*, S.A. Shaik, C.C.M. Rindt

Eindhoven University of Technology, Department of Mechanical Engineering, P.O.Box 513, Eindhoven 5600MB, The Netherlands

ARTICLE INFO

Article history:
Received 29 June 2018
Revised 11 March 2019
Accepted 13 May 2019
Available online 15 May 2019

Keywords:
Thermochemical heat storage
Potassium carbonate
TGA-DSC
Kinetics
Energy storage density
Reaction model

ABSTRACT

Thermochemical heat storage in salt hydrates is a promising method to improve the solar fraction in the built environment. One of the most promising salt hydrates to be used as thermochemical material is potassium carbonate. In this study, the use of potassium carbonate in heat storage applications is investigated experimentally. The most important objective is to form a kinetic model for the de/re-hydration reaction of the material. In order to do so, it is crucial to understand the behavior of the salt when it reacts with water vapor. Reaction kinetics and mechanism are investigated for K_2CO_3, as one of the most promising materials. Characterization of the materials is carried out with combined Thermo-Gravimetric Analysis (TGA) and Differential Scanning Calorimetry (DSC) methods. By employing the experimental results, kinetics models are developed for the hydration and dehydration reactions of the material. The kinetics model can be further used to predict the performance of a heat storage system working with K_2CO_3. In addition, cyclability and reaction enthalpy are investigated.

1. Introduction

In Europe, energy consumption for domestic purposes accounts for almost 40% of the total energy demand [1]. Therefore, a significant potential to reduce green house gas emissions exists by the reduction in fossil fuel consumption in this sector. Energy storage is a key step to shift to low carbon energy sources, which are inherently intermittent. Solar energy, as one of the most exploitable renewable energy sources, is available more than required to be harvested in residential houses during summer, while the demand cannot be met during winter. A solution is to store excess of solar energy in summer by a so-called thermal battery which can be discharged to provide heat for the residential demand in winter [2].

A promising method is heat storage using ThermoChemical Materials (TCMs), by which heat can be stored in a compact and quasi loss-free way over a long time. In the sorption heat storage process, heat is stored into an endothermal dissociation reaction (charging), and at a later time, the energy can be retrieved from the reverse exothermal reaction (discharging). In the built environment, heat generated by a solar collector during summer can be employed to desorb water from the material. The energy stored in this way can be released during winter by introducing water vapor to the dehydrated material. For low temperature sorption heat storage, adsorption of water vapor on sorption materials [3] and hydration of salt hydrates [4,5] are frequently studied. Based on theoretical energy storage density, salt hydrates (such as potassium carbonate) are better candidates compared to sorption materials (such as zeolite) [6].

In recent years, intense research has been performed on innovative system design for integrating the sorption heat storage concept into an overall system, and lab or pilot scale setups are developed and tested [7]. Several Prototypes are built based on zeolite [8,9] and some salt hydrates, such as magnesium chloride [10] and strontium bromide [11]. More studies can be found in the extensive reviews on sorption heat storage, which are done to summarize the state of the art on systems and reactors for building applications [12] and the advancements at material and prototype for long-term low-temperature applications [13].

An interesting material for thermochemical heat storage should be non-toxic, non-corrosive and stable with high energy storage density [4]. In addition, the price of the material is a crucial factor affecting the economic feasibility of a heat storage system [14]. More specifically, depending on the application, operating boundary conditions are important [5], such as hydration/dehydration temperature and vapor pressure, which are also effective on kinetics (and is directly related to power output) and deliquescence. For application in the built environment, heat storage at temperatures around 100 °C is needed, which is a obtainable temperature by usage of solar thermal collectors. A great body of material research

* Corresponding author.
E-mail addresses: m.gaeini@tue.nl (M. Gaeini), C.C.M.Rindt@tue.nl (C.C.M. Rindt).

https://doi.org/10.1016/j.enbuild.2019.05.029
0378-7788/

is available on high potential salts for temperature storage below 100 °C, such as $MgSO_4$ [15–19], $MgCl_2$ [19,20], $SrBr_2$ [21] and $CaCl_2$ [20,22,23]. In most of the available literature, some important criteria, with respect to application in the built environment, are missing while studying the salts, which will be denoted below.

Donkers et al. [5] published a review on 563 thermochemical materials in search for the most promising material for application in the built environment. A list of 25 candidates is composed first based on four criteria, i.e. energy storage density on material level above 1.3 GJ/m^3, hydration temperature above 50 °C, dehydration temperature below 120 °C and a melting point above the dehydration temperature. The list is analysed further considering additional critical parameters: Safety, chemical stability, kinetics and price. It turns out that one of the largest problems is the price. Finally, potassium carbonate (K_2CO_3) is concluded to be the best candidate among the studied material in the review. Potassium carbonate is investigated further in depth by Sögütoglu et al. [24] with respect to energy density, power output and stability, presenting a critical assessment of potential chemical side reactions in open and closed reactor concepts. It is concluded that, given the chemical robustness and the power output, 1 m^3 of material can be used with a frequency of 12–52 cycles a year (i.e. monthly to weekly), yielding a yearly basis energy of 15 – 66 GJ, which can be maintained over at least 20 years. This makes the material suitable for application in the built environment.

For thermochemical heat storage systems with application in the built environment, output temperature and power are two important parameters. For systems being used for domestic hot water production, a relatively high output temperature of at least 60 °C is required, in order to prevent bacteria growth. Although, thermal output power might drop at high temperatures [25]. Therefore, possible thermal output power from a thermochemical heat storage systems working by the material potassium carbonate needs to be investigated. Reactions occurring locally in the reactor are critical for the global performance of the system [26], such as thermal output power. Therefore, the reaction kinetics should be included mathematically in heat and mass transfer models, which are required to study such systems. Such a correlation which describes the rate equation can be estimated from kinetic analysis of the reaction. Important recommendations for performing kinetic analysis are given in the literature [27]. These recommendations are taken as a starting point to understand the concepts about chemical kinetics and the knowledge is used in the present work.

In this work, the reaction kinetics and mechanism of K_2CO_3 de/re-hydration are investigated. Characterization of the material is carried out with combined Thermo–Gravimetric Analysis (TGA) and Differential Scanning Calorimetry (DSC) methods. By employing the experimental results, kinetics models are developed for the hydration and dehydration reactions of the material. The kinetics model can be further used to predict the performance of a heat storage system working with K_2CO_3. Finally, the performance of the material is discussed based on the developed kinetics and measured enthalpy of reaction, in view of application in the built environment.

2. Materials and methods

2.1. Potassium carbonate

The interest in potassium carbonate has been sparked by its easy availability and subsequently low price (around 0.50 € /kg [28]), high capacity for water uptake and energy storage density, better chemical stability than other salt hydrates, low corrosiveness and non-toxicity. Furthermore, the material dehydrates at low temperature (below 100 °C), which makes it suitable for application in the built environment.

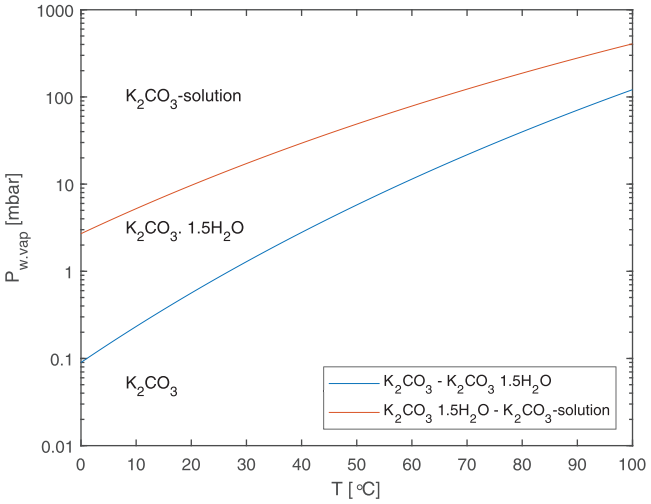

Fig. 1. Phase diagram of K_2CO_3 constructed based on Clausius–Clapeyron relation using data from literature [33].

Potassium carbonate appears as a white odorless powder. It exists in two states, namely an anhydrate state and a sequihydrate state (1.5 H_2O). The sesquihydrate occurs as small, white, translucent crystals. At room temperature, it has an equilibrium relative humidity of approximately 43% [29]. It reaches to a deliquescent state when left open to room atmosphere, so proper storing of the material is critical. The following equation describes the reversible hydration-dehydration reaction for potassium carbonate.

$$K_2CO_3 \cdot 1.5\ H_2O(s) \underset{Heat\ Extracted}{\overset{Heat\ added}{\rightleftharpoons}} K_2CO_3(s) + 1.5\ H_2O(g). \quad (1)$$

On heating a sesquihydrate form of potassium carbonate ($K_2CO_3 \cdot 1.5\,H_2O$), it dissociates to anhydrous form (K_2CO_3) and water vapor, leading to an endothermic reaction. When the anhydrous form reacts with water vapor, it forms a sesquihydrate leading to an exothermic reaction. It is a single step reaction leading to a simple kinetic mechanism. The only stable states of hydration reported in literature [5,24,30,31] and experimentally observed in the present work are the anhydrate and sesquihydrates forms.

In order to perform hydration-dehydration reactions, it is important to understand the thermodynamic properties of the salt hydrate. Using the concept of reversible reactions, heat can be extracted. In real life, a thermal storage system can be designed using the concept. However, in order to actually utilize the concept, it is necessary to control the operating conditions such as water vapor pressure and temperature. For K_2CO_3, these conditions can be retrieved from the constructed phase diagram based on thermodynamics properties as shown in figure Fig. 1. The phase diagram can be constructed using the Clausius–Clapeyron equation [32]:

$$\frac{d\ln(P_{eq})}{d(1/T)} = \frac{\Delta h}{R} \quad (2)$$

where P_{eq} [Pa] is the equilibrium water vapor pressure between the two hydrate phases, T[K] is the corresponding temperature, R [J/kg/K] is the gas constant and Δh [J/mol] is the reaction enthalpy per mole of H_2O.

In Fig. 1, the blue line represents the equilibrium line between the two states of hydration of potassium carbonate ($K_2CO_3 \cdot 1.5\,H_2O$ – K_2CO_3). The equilibrium vapor pressure P_{eq}[Pa] is fitted by:

$$P_{eq} = 4.228 \times 10^{12}\, exp\left[-\frac{7337}{T}\right] \quad (3)$$

where T [K] is temperature. The ratio between water vapor pressure (P_w) and equilibrium water vapor pressure (P_{eq}), called the pressure ratio ($= P_w/P_{eq}$), is an important parameter in reaction kinetics. To find out the pressure ratio, the equilibrium water vapor pressure can be calculated from Eq. (3) and the actual water vapor pressure is known from experimental conditions.

During the hydration process, after a certain state of hydration liquefaction (deliquescence) occurs, which is caused by the depression of the melting point upon water uptake. This is caused by the highly hygroscopic nature of the material. In Fig. 1, the red line represents the deliquescence transition. In practice, this means the formation of an aqueous solution instead of a solid state material. Dehydration of such an overhydrated solution yields an agglomerated bulk of solid material, instead of the initial powdery porous form. Agglomeration is an undesirable behavior of the material, because it prevents or decelerates the subsequent water uptake process [23]. Therefore, the operation condition should be chosen such to avoid overhydration. By controlling the conditions in an experiment, as well as in a storage system, it becomes possible to stay below the deliquescence line.

The material used in this study is the pure salt (Sigma–Aldrich) in powder form (500 – 1000 μm particles) and the state of hydration for the material in the container is 1.5 moles of water per mole of potassium carbonate (sesquihydrate $K_2CO_3 \cdot 1.5\,H_2O$). However, due to the hygroscopic nature of the material, the water uptake after being taken out of the container and exposed to room conditions is fast. Since the initial state of hydration is generally unknown for a sample, the experiments are always started with an initial dehydration cycle (at a temperature of 100 °C).

2.2. TGA-DSC setup

The characterization of TCM is based on measurement data, obtained through the methods of Thermo–Gravimetric Analysis (TGA) and Differential Scanning Calorimetry (DSC). A Simultaneous Thermal Analysis (STA) apparatus (Netzsch STA 449 F3 Jupiter) connected to a Modular Humidity Generator (MHG ProUmid) is used, which allows for simultaneous measurement of both the mass change (TGA) and the heat release/uptake (DSC) of a sample. The STA apparatus consists of a thermally controlled environment (furnace), which is subjected to a pre-defined temperature program. The sample is situated in an aluminium crucible located in the furnace, with a typical sample mass of around 10 mg. An empty crucible is located just beside the sample crucible as reference for the DSC measurement. The crucibles are assumed to be subjected to identical conditions. Both crucibles are positioned on a sample holder, which is mounted on top of a balance. The humidity generator provides an air flow with a controlled flow rate, temperature and humidity. The air flow is from top to the bottom of the furnace. A schematic view of the setup is shown in Fig. 2.

The TG signal shows the weight change of a sample during an experiment with respect to the initial mass, as measured with the balance. The temperature of each crucible is measured with a thermocouple attached at the bottom of each platform on which the respective crucible is situated. The temperature difference between the sample crucible and the neighbouring reference crucible is recorded. The temperature difference serves as a measure for the heat flux towards or from the sample. The DSC signal is a measure for the heat flow to or from the sample: negative values indicate exothermic reactions, positive values indicate endothermic reactions; the direction of exothermic values is indicated on the respective axis. Generally, hydration and thus mass gain, implies an exothermic reaction, whereas dehydration implies an endothermic reaction.

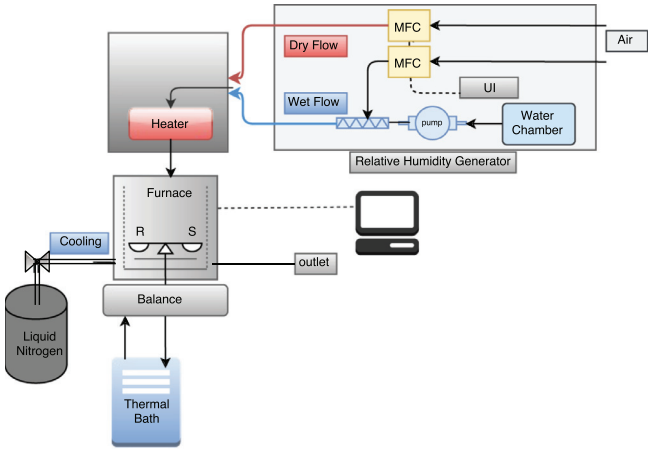

Fig. 2. Schematic view of TGA-DSC setup.

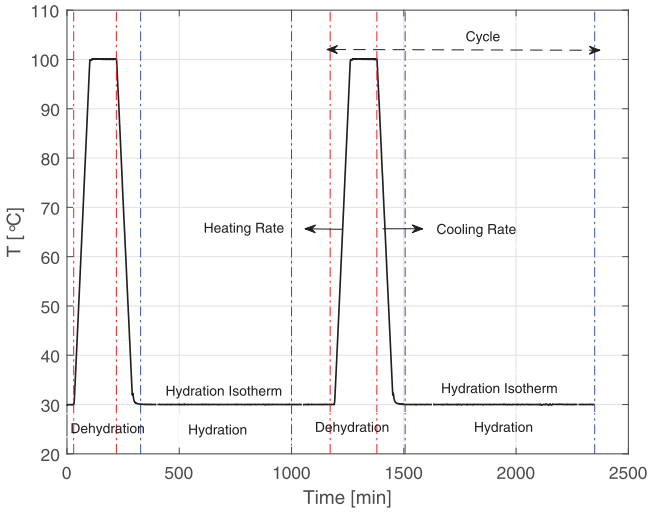

Fig. 3. Temperature program used in the experiments.

2.3. Experimental conditions

The typical experiments are conducted in an air atmosphere with a flow rate of 500 ml/min. A sample of $K_2CO_3 \cdot 1.5\,H_2O$ is first dehydrated in a dry air atmosphere with a heating rate of 10 K/min from the ambient temperature to 100 °C. Afterwards, the furnace is cooled down to the ambient temperature and kept at this temperature. Then humid air is introduced to the furnace in order to hydrate the sample. In this work, the reference water vapor pressure of 13 mbar is chosen, being the saturation water vapor pressure at 10 °C, which is a typical borehole (humidity generator) temperature in the Dutch climate [10].

The temperature program used in the experiments is shown in Fig. 3. The initial heating is implemented for the sample to completely dehydrate and reach anhydrous state at a maximum temperature of 100 °C. Also, through the course of the experimentation, a cycling effect was observed; as hydration reaction becomes faster after each cycle till a certain number of cycles. The experimental data used in the analysis are from the cycles where there is no further cycling effect.

Table 1 shows the experimental conditions used for de/re-hydration experiments. While performing these experiments, all the other half-cycles in between are of similar conditions (typical experiment), in order to avoid any after effects due to different

Table 1
Experimental conditions for de/re-hydration experiments.

Operating parameter	Dehydration	Rehydration
Initial temperature (°C)	27–30	27–30
Dehydration temperature (°C)	26–57	85–150
Water vapor pressure (mbar)	8.4–17.5	0.3-2.5
Heating/cooling rate (K/min)	10	0.5–20
De/re-hydration time (min)	15–300	40–120

experimental conditions of preconditioning as observed by Stanish and Perlmutter [31].

2.4. Evaluation of reaction kinetics

The rate of conversion of a reaction can be generally described by the following equation [27,34,35]:

$$\frac{d\alpha}{dt} = k(T)\cdot f(\alpha)\cdot h(p)$$
$$\frac{d\alpha}{dt} = A_f \cdot exp\left(-\frac{E_a}{RT}\right)\cdot f(\alpha)\cdot\left(\frac{P_w}{P_{eq}}\right) \quad (4)$$

where $k(T)$ is the temperature function which is an Arrhenius type function. This function contains the activation energy E_a[J/mol], pre-exponential factor A_f[1/min] and the gas constant R [J/kg/K]. $f(\alpha)$ is the conversion function or the reaction model, where α is the extent of conversion. Finally, $h(p)$ is the pressure function, which is usually the ratio between the water vapor pressure and the equilibrium pressure.

In order to evaluate the performance of the materials, TG and DSC signals can be converted to performance indication factors, such as loading (or state of hydration), conversion, conversion rate, and reaction enthalpy.

The loading L, or state of hydration, is the number of water molecules N_{H_2O} per number of potassium carbonate crystal units $N_{K_2CO_3}$, and can be calculated by:

$$L = \frac{N_{H_2O}}{N_{K_2CO_3}} = \frac{m_{H_2O}/M_{H_2O}}{m_{K_2CO_3}/M_{K_2CO_3}} \quad (5)$$

where m_{H_2O} is the mass increase of the sample starting from the anhydrous state due to the absorption of water, and $m_{K_2CO_3}$ is the mass of the anhydrous salt, and M_{H_2O} and $M_{K_2CO_3}$ are the molar mass of water and potassium carbonate, respectively. The anhydrous state is recognized when the TG signal is more or less constant in time at high temperatures.

The conversion of dehydration (deH) and rehydration (reH) reactions are calculated based on the TG signal α, which can also be presented based on loading as:

$$\alpha = \frac{L - L_i}{L_f - L_i} = \begin{cases} (1.5 - L)/1.5 & ,deH \\ L/1.5 & ,reH \end{cases} \quad (6)$$

where L is the loading at a certain moment in time, and L_i and L_f are the initial and final loading values, respectively.

The enthalpy of reaction is determined through the energy change during a reaction. The stoichiometry of the reaction itself is identified through the mass change, and is used to calculate the change of state of hydration. The reaction enthalpy is the energy released or absorbed per mole of water and can be obtained by:

$$\Delta h = \frac{\Delta H}{N_{H_2O}} \quad (7)$$

where ΔH is the released heat, as measured in the STA apparatus, which can be calculated by integrating the heat flow over the course of a reaction, according to:

$$\Delta H = \int_{t_i}^{t_f} [DSC(t) - BL(t)]dt = \int_{t_i}^{t_f} \dot{Q}dt \quad (8)$$

The DSC signal shows the power with which the heat is adsorbed (in endothermic reaction of dehydration) or released (in exothermic reaction of hydration) by the sample. In theory, the baseline (BL) should have a value of approximately zero. The deviation of the DSC signal from the baseline indicates the occurrence of a chemical process, involving thermal effects.

The reaction rate (presented in Eq. (4)) is used in the fitting procedure through the experimentally calculated reaction rates. In the implemented fitting, unknown parameters are determined such that residual sum of squares. The reaction rate equation is rewritten based on the fitting parameters as:

$$\frac{d\alpha}{dt} = [Y(1)].(1-\alpha)^{[Y(2)]}.\left(\frac{P_w}{P_{eq}}\right)^{[Y(3)]} \quad (9)$$

where $[Y(1)]$, $[Y(2)]$ and $[Y(3)]$ are the fitting parameters for the rate constant $k(T)$, reaction order n and order of the pressure ratio term, respectively.

3. Results

Different samples are investigated through the water adsorption and energy exchange of the materials during de/re-hydration reactions, which are measured by the TGA and DSC methods. In this section, results of typical experiments are presented, firstly. Secondly, dependencies on the sample mass and cycling are investigated. Then, kinetics models for hydration and dehydration are developed. Finally, the reaction enthalpy is studied.

The sample mass, used in the figures and tables, represents the mass of the active material in a sample (dry potassium carbonate content), which would be the sample mass after the first dehydration. In addition, the salt content of each sample can be determined using the experimental results, by comparing the calculated equilibrium loading based on measurements and the theoretical equilibrium loading from Fig. 1. This method gives results that are accurate with in one percent.

3.1. Typical experimental results

A typical experimental result is shown in Fig. 4. A sample of $K_2CO_3 \cdot 1.5\,H_2O$ is first dehydrated in a dry air atmosphere in the apparatus. The temperature increases firstly from 26 °C to 100 °C with a heating rate of 10 K/min (red dotted line). Afterwards the furnace is cooled down to 26 °C and kept at this temperature (blue dotted line). Then humid air with a water vapor pressure of 13 mbar is introduced to the furnace in order to rehydrate the sample. The TG and DSC signals are shown vs. time in Fig. 4(a) and (b), respectively.

As can be observed in Fig. 4(a), during dehydration, the sample loses mass (red solid line), indicating the desorption of water molecules from the salt crystal structure and eventually reaches to the complete anhydrous state, as the TG signal is constant. When the humidity is introduced to the furnace during hydration, the sample gains mass again (blue solid line).

In the measured DSC data (Fig. 4(b)), negative values indicate an endothermic process (dehydration) and positive values indicate an exothermic process (hydration). The direction of exothermic signal is indicated on the respective axis. The TG signal can be related to the DSC signal as rate of mass change corresponds to the rate of heat flux to or from the sample. The step changes in TG signal corresponds to energy peaks in the DSC signal. As water molecules are desorbed from the sample during dehydration, a mass loss is seen in TG signal leading to energy storage in the sample observed as a negative peak in DSC signal. Conversely, as water molecules are absorbed by the sample during hydration, a mass gain is seen in TG signal, consequently, leading to release of energy observed as a positive peak in DSC signal.

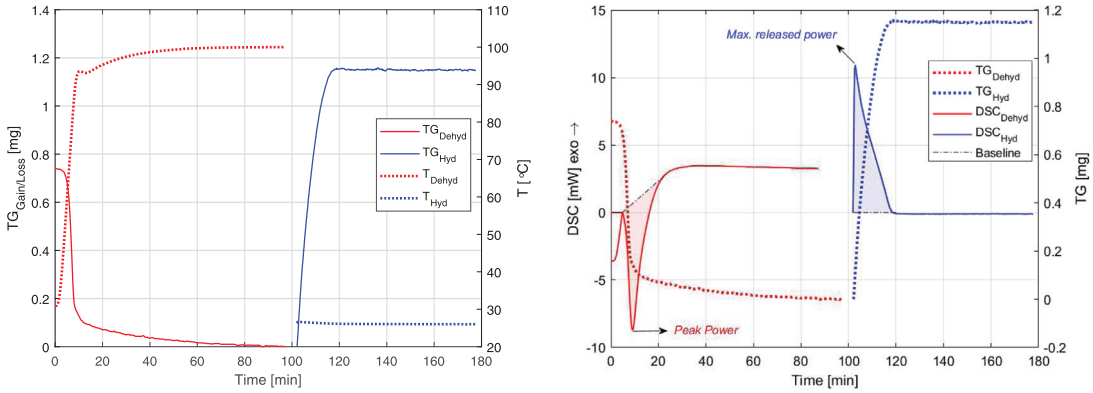

(a) TG signal (b) DSC signal

Fig. 4. Typical result of a 8mg $K_2CO_3 \cdot 1.5\,H_2O$ sample subjected first to dehydration in dry air atmosphere with a heating rate of 10 K/min from 26 °C to 100 °C, and then subjected to rehydration in a humid air atmosphere with a water vapor pressure of 13 mbar and a temperature of 26 °C.

In Fig. 4(b), blue and red shaded regions indicate the integrated area, which represent the released and stored energies during the hydration and dehydration reactions, respectively. Also, the peaks show the maximum power required for dehydration and released during hydration. Since the released power during hydration reaction directly translates to a power output, it is an important parameter while varying different experimental parameters [35], and will be discussed further in Section 4.

The extent of conversion can be calculated based on TG signal by Eq. (6), and then reaction rate can be calculated by derivative of the conversion over time. Fig. 5 shows the conversion and reaction rate vs. time for the experiment presented above. For both hydration and dehydration, conversion is changing from 0 at the beginning to 1 at the end of the reactions. For dehydration, reaction rates start from a minimum and then reach a maximum value, because the sample loses mass when the temperature is ramped up, as seen in the temperature profile. Whereas for hydration, the reaction rate (rate of conversion) is maximum at the start of the reaction (at around t = 100 min as indicated in the figure), as soon as humid air is introduced to the system.

For all the experiments so forth, the same procedure is followed to calculate the conversion and reaction rates for both hydration and dehydration.

3.2. Sample mass in-dependency

The mass of sample is an important parameter regarding kinetics [23]: During hydration, the diffusion of vapor through the sample is limited for large samples; and during dehydration, temperature distribution over the sample is not uniform for large samples, which leads to limited reaction rate in the core of the sample. Therefore, a set of experiments is performed to identify a suitable range of sample mass at which the effects are minimum.

In addition, the temperature of the reference program used in the experiment should be similar to temperature of the sample under investigation. There is difference between the former and latter on two occasions: the first being the usage of high heating rates and the second when large sample masses are used. Both cause undesirable thermal effects which give an error in kinetic parameter estimation [27]. In order to avoid the undesirable thermal effects, sample mass in-dependency experiments are performed.

Fig. 6 shows the results for hydration reaction rate of samples with various masses vs. time. Samples with large masses exhibit slower reaction rates. The curves of samples with mass of 9 and 10 mg show similar reaction rates. Hence, a sample mass of around 10 mg can be used in experiments, so the experimental results are independent of the sample mass.

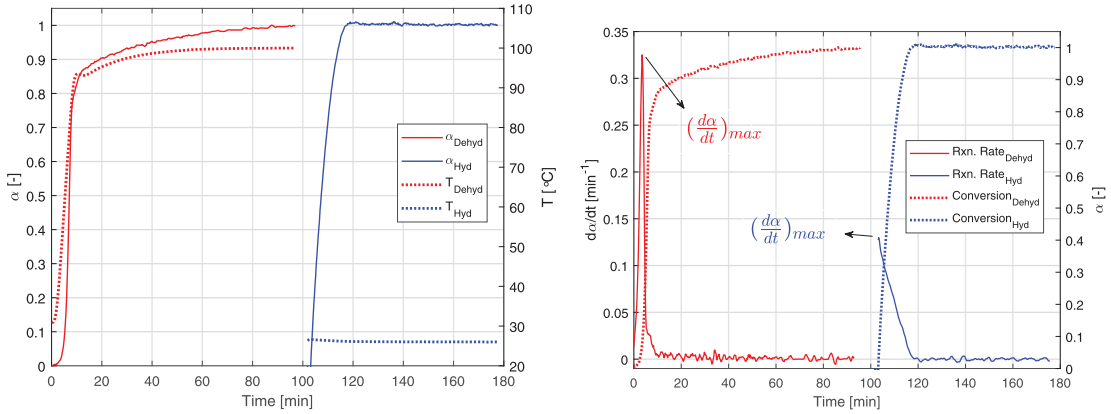

(a) Extent of conversion (b) Reaction rate

Fig. 5. Extent of conversion and reaction rate calculated for the experiment shown in Fig. 4.

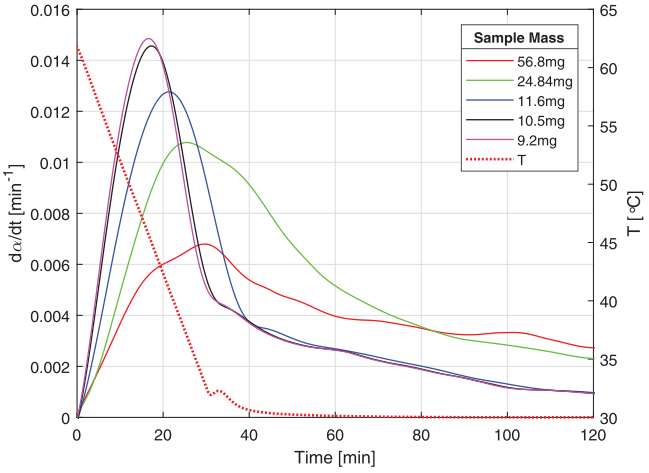

Fig. 6. Hydration reaction rates as a function of time for various initial sample masses.

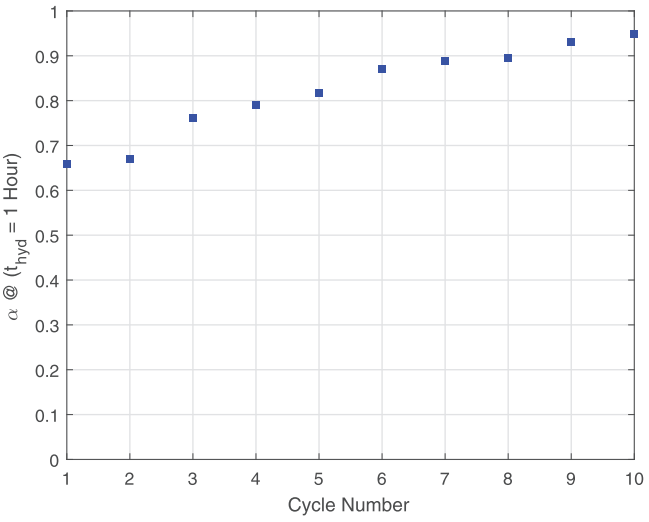

Fig. 7. Extend of conversion after 1 h for 10 hydration-dehydration cycles of a 10 mg sample. Typical conditions (as presented in Section 2.3) are applied for hydration and dehydration.

3.3. Cyclability

Cyclability of thermochemical materials is one of the most important features to be considered, since a system should be able to work through multiple cycles in order to be feasible. Performance of the materials usually degrades over cycles. Especially, in case the deliquescence phenomenon occurs during hydration of the material, porous structure of the material will be lost, which leads to a degradation in performance. The cyclability of potassium carbonate is studied in this section.

Fig. 7 shows extend of conversion of hydration after 1 h for 10 hydration-dehydration cycles of a potassium carbonate sample. As can be seen, the extend of conversion is increased in each cycle compared to the previous one. Therefore, performance of potassium carbonate improves over cycles, and its kinetic becomes faster after each cycle. Based on observation, the volume of the sample increases after each cycle, which can be the explanation for the improvement in performance. After each hydration, the crystal expands as expected, because of placement of water molecules in its structure. During subsequent dehydration, water molecules are removed from the structure, but the powder is not contracted to the original form. Therefore, the porosity of the sample is increased. Higher porosity ease the vapor transport through the sample, and hence, speed up the kinetics. This phenomenon happens till the sample reaches a certain openness, and then stays the same. The experiments presented in the following sections are with the samples which are stabilized through cyclic preconditioning.

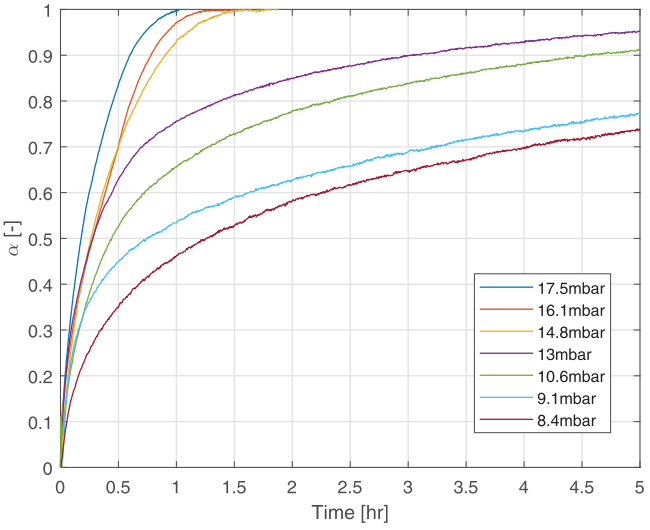

Fig. 8. Hydration Conversion plotted as a function of time at a hydration isotherm of 30 °C for various water vapor pressure P_w using an initial sample mass of 10 mg.

3.4. Hydration kinetics

The following section presents the results of hydration experiments with operating conditions presented in Section 2.3. Different parameters are varied to investigate effects on reaction rate. Finally, a kinetic parameter estimation is done and a numerical model is constructed based on the experimental results.

3.4.1. Effect of water vapor pressure

A set of experiments is designed to see the influence of the vapor pressure on the kinetics. In these experiments, the hydration isotherm is kept at 30 °C and hydration is only started when water vapor is introduced to the system while the isotherm temperature is maintained. The water vapor pressure (P_w) is varied for each hydration cycle using the humidity generator.

Fig. 8 shows the effect of water vapor pressure on the hydration conversion. It can be observed that hydration of K_2CO_3 has an expected dependency with regard to vapor pressure; conversion is faster for experiments with higher water vapor pressure. This implies that with higher vapor pressure, there is more driving force to complete the hydration process.

To identify a relationship between reaction rate and water vapor pressure, Fig. 9 is plotted. It shows the relation between average (Fig. 9(a)) and maximum (Fig. 9(b)) reaction rate with respect to the pressure ratio (P_w/P_{eq}). The equilibrium pressure (P_{eq}) is known from the phase diagram of K_2CO_3 (Fig. 1 and Eq. (3)). The important finding is that the overall reaction rate is directly proportional to the vapor pressure, hence a linear relationship is established. Applying higher pressure ratios means having high water vapor pressure values away from the equilibrium line, as seen in the phase diagram of K_2CO_3, which leads to faster reaction rates.

In order to have a uniform spread of values, the average rate is taken over an uniform time interval for all the cases. From the obtained results, Eq. (10) shows that reaction rate for hydration of K_2CO_3 follows a linear dependence with water vapor pressure ratio. This is further confirmed with the kinetics parameter estima-

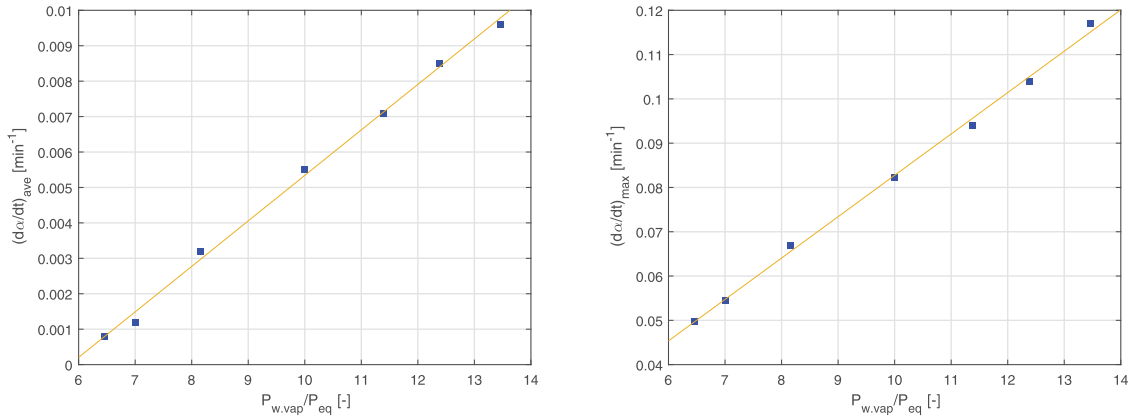

(a) Average hydration reaction rate (b) Maximum hydration reaction rate

Fig. 9. Hydration reaction rate versus pressure ratio at a hydration isotherm of 30 °C using an initial sample mass of 10 mg.

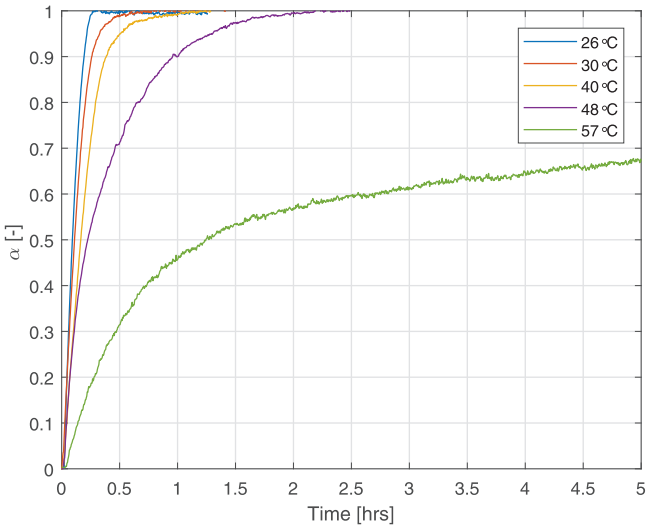

Fig. 10. Conversion vs. time for hydration at various hydration isotherms with vapor pressure of 13 mbar using an initial sample mass of 8*mg*.

tion presented in Section 3.4.4.

$$\frac{d\alpha}{dt} \propto h(p) = \frac{P_w}{P_{eq}} \tag{10}$$

3.4.2. Effect of temperature

A set of experiments is designed to identify the effect of temperature on the reaction rate. This way, it can be found out if the hydration reaction of potassium carbonate follows an Arrhenius type of temperature dependency as presented in Eq. (4). The experiments were carried out at a fixed water vapor pressure P_w of 13 mbar.

Fig. 10 shows conversion of hydration reaction vs. time for different isothermal temperatures. As can be seen, higher temperature leads to slower reaction. The reason is that the higher temperatures T_{eq} are closer to the equilibrium temperature. The equilibrium temperature is the temperature at which, for a specific vapor pressure, the two phases (anhydrous and sesquihydrate) are in equilibrium, and hardly any conversion from one phase to another one happens. The equilibrium temperature for the 13 mbar vapor pressure can be seen in the phase diagram Fig. 1 as the blue curve. From the phase diagram, it can be seen that the equilibrium temperature for a vapor pressure of 13 mbar is equal to 60 °C. Here, the higher temperatures are closer to the equilibrium temperature (in this case T_{eq} =60 °C for a vapor pressure of 13 mbar), which leads to slower reactions. Having point of operation in the region close to the equilibrium line leads to a low reactivity.

Fig. 12 shows the range of maximum reaction rates obtained by varying vapor pressures and isotherms for K_2CO_3 from the different experiments performed for hydration.

Fig. 11(a) shows the reaction rate plotted against extent of conversion. Clear peaks exist once the hydration is started ($\alpha = 0$). In order to find the Arrhenius dependence of the reaction rate, average and maximum reaction rates are plotted in Fig. 11(b). It can be seen that at higher temperatures, the reaction rate proceeds very slowly. However, the trend is not as clear for the average reaction rates as the maximum reaction rates.

From the Arrhenius law, it is known that as temperature is increased, the rate constant ($k(T)$ as presented in Eq. (4)) increases, which ultimately increases the reaction rate. However, the results here show that with the increase in temperature, the reaction rate decreases. The Arrhenius dependence needs to established after finding out the values of individual rate constants for these experiments. This is done in Section 3.4.4.

3.4.3. Shape of reaction model

As mentioned earlier, the hydration of potassium carbonate follows a single step reaction. The procedure to obtain an appropriate reaction model for a single step reaction is stated in the work of Vyazovkin et al. [27]. The single-step model can be selected by a variety of numerical and graphical methods.

It is stated in the work of Vyazovkin et al. [27], that when the reaction rate is at its maximum value as soon as the sample reaches the isothermal temperature, then the reaction is decelerator. Models of the decelerating type represent processes whose rate has maximum rate at the beginning of the process and decreases continuously as the extent of conversion increases. A similar behavior for the hydration of K_2CO_3 is observed in Fig. 11(a), where the hydration process has maximum rate at the beginning of the conversion. The most common example of a decelerator reaction model is,where n is the reaction order:

$$f(\alpha) = (1-\alpha)^n \tag{11}$$

Fig. 13 shows the plot ln(1 - α) vs. time for the conversion values obtained from the results presented in Fig. 10. After analyzing the shape of the plot from Fig. 13, the first order reaction ($n = 1$) and contracting sphere ($n = 2/3$) models are possible for hydration of K_2CO_3, which are the first-order reaction model and the contracting volume reaction model, respectively. However, a more ex-

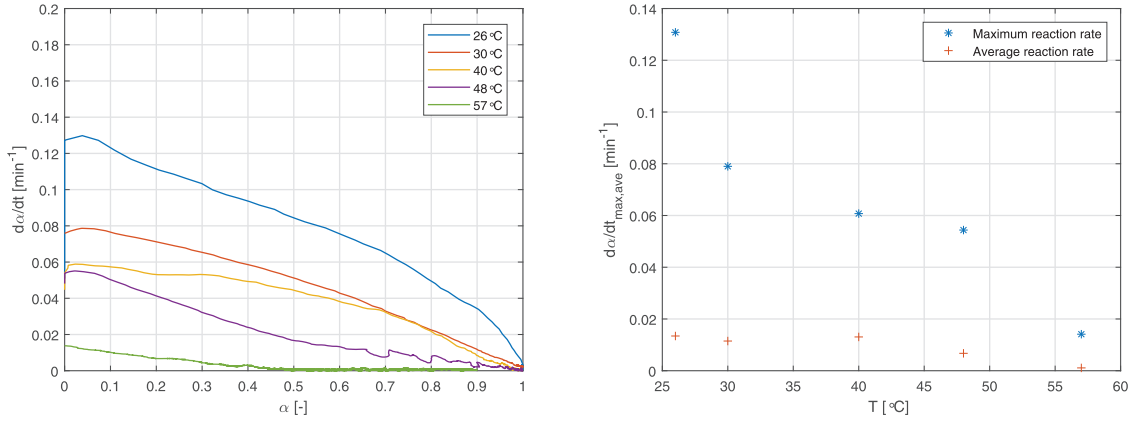

(a) Rate vs. conversion (b) Maximum & average rate vs. T

Fig. 11. Hydration reaction rate vs. conversion and temperature at a water vapor pressure of 13 mbar.

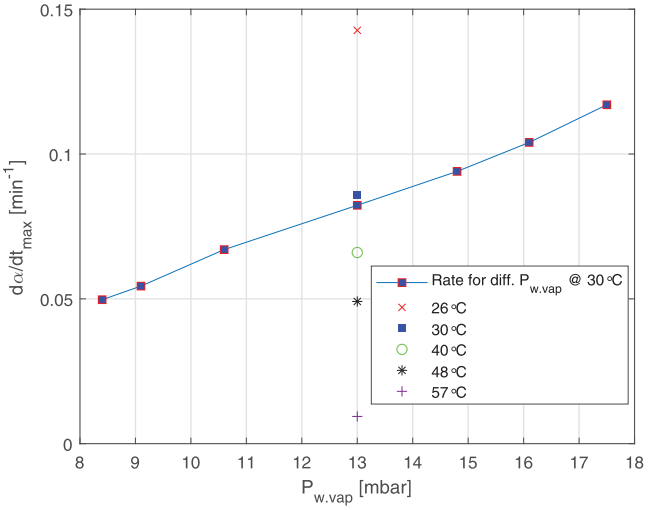

Fig. 12. Reaction rate variation with respect to changes in hydration isotherms and vapor pressure.

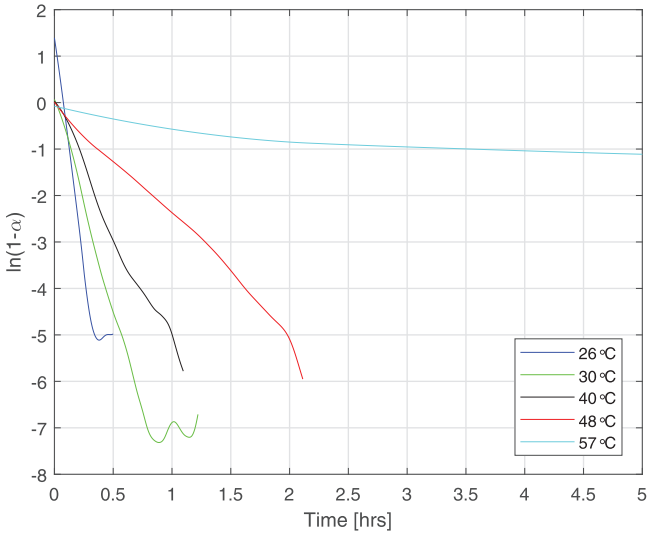

Fig. 13. ln(1 - α) vs. time plot to identify reaction models $f(\alpha)$.

Table 2
Fitting parameters in the rate equation.

T_{iso} [°C]	[Y(1)]	[Y(2)]	[Y(3)]
26	0.67 x 10^{-2}	0.66	1.0024
30	1.67 x 10^{-2}	0.6552	0.9824
40	2.21 x 10^{-2}	0.6529	0.9929
48	2.94 x 10^{-2}	0.6706	0.9848

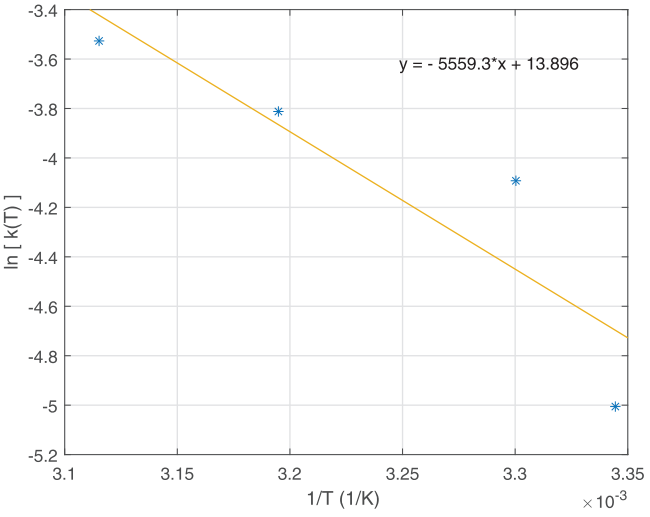

Fig. 14. Arrhenius Plot values for Hydration of K_2CO_3.

act value of n is attempted to be found out from the model fitting method in the following section.

3.4.4. Estimation of parameters

As presented in Section 2.4, the reaction rate is fitted with Eq. (9) and results are presented in Table 2. The fitting parameters [$Y(1)$], [$Y(2)$] and [$Y(3)$] are the rate constant $k(T)$, reaction order n and order on the pressure ratio term respectively.

The parameter Y(1) gives the rate constant $k(T)$ for the different hydration isotherms. Once the rate constants $k(T)$ is known, the Arrhenius parameters, activation energy E_a and exponential pre-factor A_f are obtained from Fig. 14 and presented in Table 3, by constructing a reordered Arrhenius equation:

$$ln(k(T)) = -\left(\frac{E_a}{R}\right).\left(\frac{1}{T}\right) + ln(A_f) \quad (12)$$

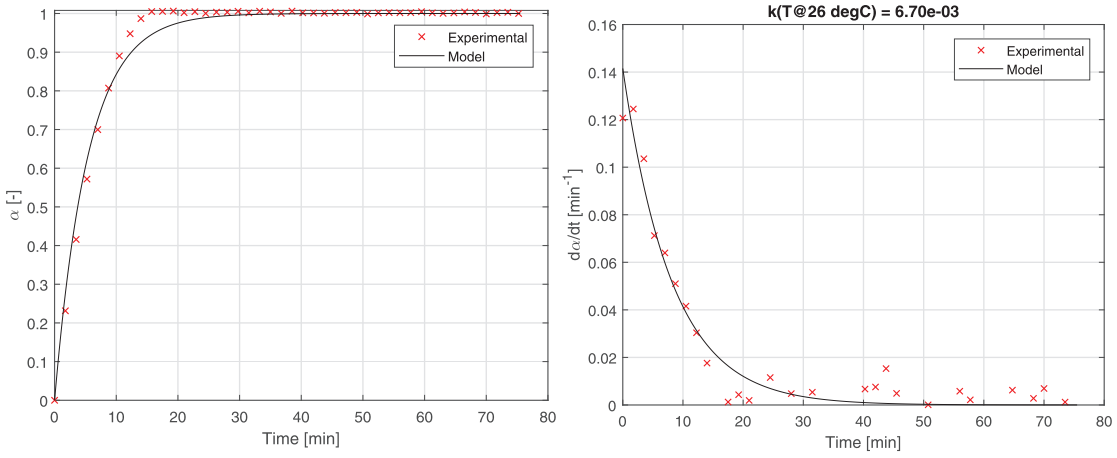

(a) Conversion (b) Reaction Rate

Fig. 15. Comparison between experimental data and numerical kinetic model data for hydration at isotherm temperature of 26 °C.

Table 3
Kinetic parameters for hydration of K_2CO_3.

	$E_{a,hyd}$ [kJ/mol]	$A_{f,hyd}$ [1/min]
Hydration	46.220	1.0838×10^6

Table 4
Arrhenius law validation for hydration experiments performed with different hydration isotherms.

T_{iso}[°C]	k [1/min]	P_w/P_{eq} (-)	R^2
26	0.0067	16.25	0.97
30	0.0167	10	0.98
40	0.0221	5.41	0.97
48	0.0294	2.7	0.96

It can be seen from Table 2 that the order of reaction model n (parameter Y(2)) takes up a power of approximately 0.66, which represents a contracting sphere model ($f(\alpha) = (1-\alpha)^{2/3}$). In addition, the dependency on the pressure ratio is found to be linear ($Y(3) \approx 1$).

Table 4 shows the values of rate constants and the pressure ratios, which are used in the hydration experiments for various hydration isotherms. It is observed that as the temperature increases, the rate constant also increases which validates the Arrhenius law. However, as seen in Fig. 11(b), reaction rates are slower for higher temperatures. This is explained by the pressure ratio values as seen in Table 4, which decrease by increasing temperature.

3.4.5. Final hydration reaction model

To conclude, the kinetics of hydration reaction of K_2CO_3 can be modelled using Eq. (13) with the kinetic parameters in Table 3. The experimental data for each isotherm temperature is comparable with mathematically constructed reaction rate. Table 4 shows their corresponding R^2 values determining the accuracy of the fit. The values are close to 1 indicating the model to be a good fit for the experimental results.

$$\frac{d\alpha}{dt} = A_f \cdot exp\left(-\frac{E_a}{RT}\right) \cdot (1-\alpha)^{2/3} \cdot \left(\frac{P_w}{P_{eq}}\right) \tag{13}$$

As an example, Fig. 15 shows the comparison between the experimental and numerical kinetics model data for the isotherm at 26^oC. The model predicts the extent of conversion to an acceptable degree of accuracy, however at the point of completion of reaction, the model underestimates the conversion.

The numerically obtained reaction rates and conversions using Eq. (13) are shown in Fig. 16, for all the isotherm temperatures.

3.5. Deydration kinetics

The following section presents the results of dehydration experiments with operating conditions presented in Section 2.3. Different parameters are varied to investigate effects on reaction rate. Finally, a kinetic parameter estimation is done and a numerical model is built based on the experimental results.

3.5.1. Effect of water vapor pressure

Similar to the hydration experiments, the dehydration driving force is investigated. Using the relative humidity generator device, the water vapor pressure is changed. For a favorable dehydration cycle, the P_w should be close to 0 mbar. In reality, it is not possible to attain a 0% R.H. in the experimental environment. The minimum attainable R.H. value in the apparatus is 1.1%, which corresponds to 0.3 mbar water vapor pressure. The aim of these experiments is to vary the vapor pressure, in order to understand the dependency of reaction rate to pressure ratio. Fig. 17 shows the results for dehydration of K_2CO_3. The sample is heated up to 100 °C with a heating rate of 10 [K/min], as seen in the temperature profile in Fig. 17(a).

It can be observed that as the vapor pressure is increased, the conversion slows down. In order to validate this, the reaction rates are plotted against the pressure ratios. Fig. 17(b) shows that as pressure ratio increases, the reaction rate decreases. According to the literature [30], similar experimental results have been observed, that is, when the pressure ratio (P_w/Peq) approaches to 1, reaction rates becomes closer to zero. Analogous to the case of hydration, it can be concluded that the pressure function is also a driving force for dehydration. For dehydration of K_2CO_3, reaction rate is inversely proportional to water vapor pressure.

3.5.2. Effect of temperature

A set of experiments is designed to identify the effect of temperature on the reaction rate. The dehydration is carried out while heating up from ambient temperature to different temperatures using a constant heating rate of 10 [K/min]. The expected result is that a trend could be achieved when temperature is varied similar to the hydration process.

Fig. 18(a) shows the conversion for dehydration reaction when heating up a sample to different temperatures. No expected trend

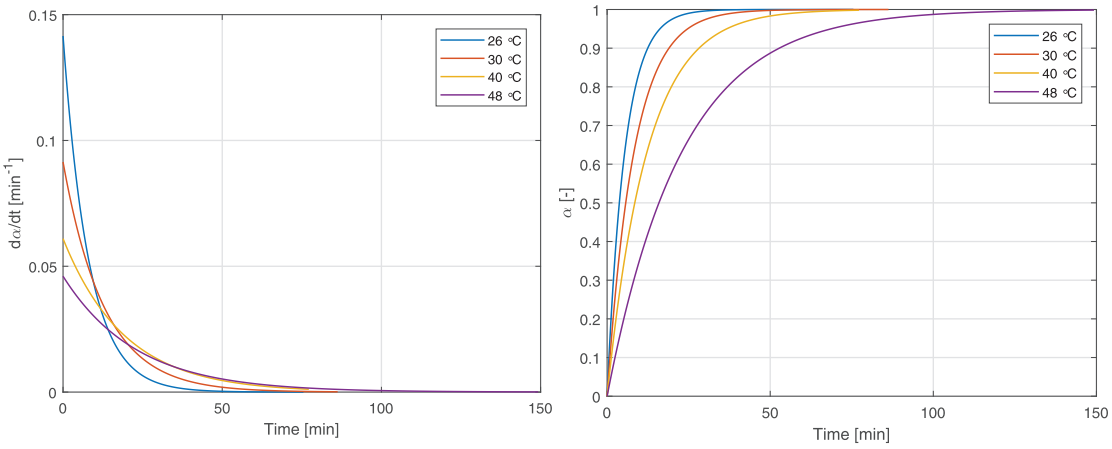

(a) Reaction rate (b) Conversion

Fig. 16. Numerically modelled reaction rates and conversions for various hydration isotherms.

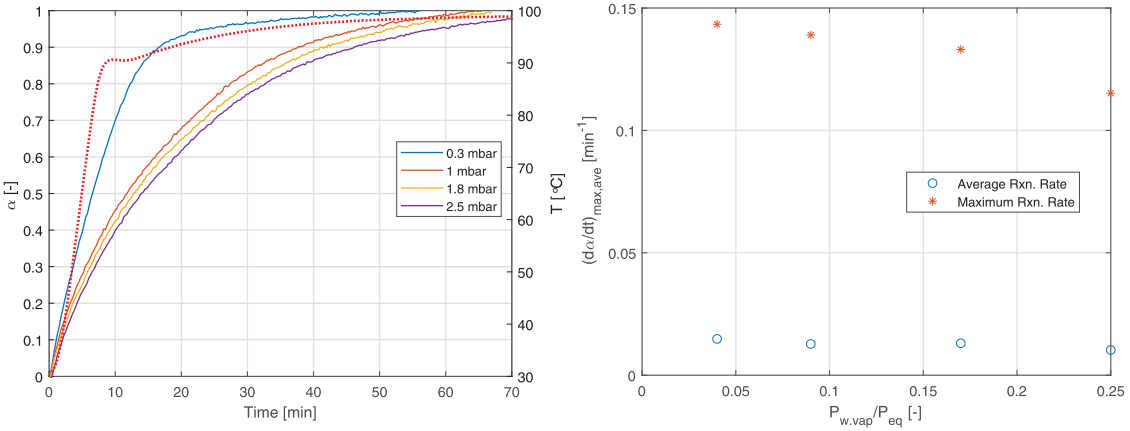

(a) Conversion versus time (b) Reaction rates versus pressure ratios

Fig. 17. Effect of water vapor pressure on conversion and reaction rates for dehydration of a sample with an initial mass of 8 mg. The heating rate used is 10 [K/min] and the temperature profile can be seen in **(a)**.

is observed, moreover, all the conversion curves have almost the same completion time. Fig. 18(b), that shows the reaction rates, also does not show a particular trend. This is because the dehydration process is completed in the heating up ramp, from the initial start temperature to the final set temperature as seen in Fig. 18(a), where the dotted lines show the temperature profiles. Irrespective of the final temperature, dehydration starts as soon as an appropriate driving force is available with increase in temperature. So, even before the final isotherm is reached, most of the dehydration reaction is completed.

Since dehydration occurs at a non-isothermal temperature condition, as opposed to hydration, the procedure to obtain kinetics for dehydration will differ from the procedure used for hydration. The use of single heating rate methods for the purpose of kinetic predictions of dehydration experiments is not capable of producing meaningful results [27], so multiple temperature programs are used. Iso-conversional methods will be used, which employs the use of different heating rates to investigate the dehydration process.

3.5.3. Effect of heating rate

A set of experiments is designed to investigate dehydration process with varying heating rates with a final temperature of 100 °C and a vapor pressure 13 mbar. Dehydration is an endothermic reaction, which is related to the amount of heat provided per unit of time, and is exactly the function of heating rate.

Fig. 19 shows the dehydration conversion and reaction rate for various heating rates. It can be clearly observed that conversion is faster for higher heating rates. For higher heating rates, more amount of heat is provided per minute, leading to a faster conversion and higher reaction rate. This data will be used for kinetic model prediction for dehydration of K_2CO_3.

3.5.4. Estimation of parameters

In order to utilize the isoconversional methods, peak temperatures T_{max} (the temperature at which the rate is maximum) are needed to be retrieved from the DSC/DTG signals of the experiments. Fig. 20 shows the peak temperatures for each heating rate, for both the differential scanning calorimetry (DSC) signals as well as derivative thermo–gravimetric (DTG) signals. The DSC signals only for this set of experiments were recorded with the values being positive for dehydration.

For the DSC signals, T_{max} is retrieved from the curves at the point where the difference is maximum relative to the baseline of the curve. In this manner, peak temperatures extracted from DSC and DTG are listed in Fig. 20(a) and (b), respectively. Peak temperatures from both the signals are almost equal with not much drastic differences, as expected.

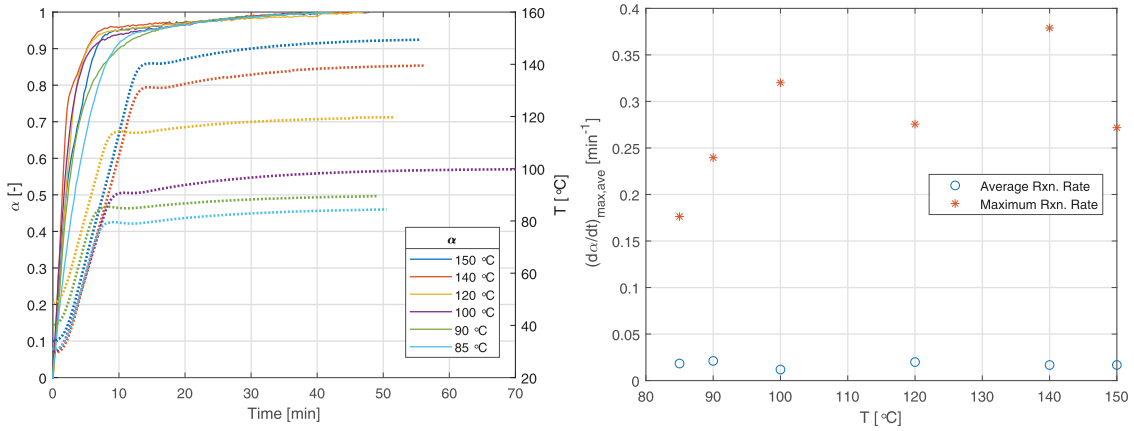

(a) Conversion for various final temperatures (b) Reaction rates versus final temperature

Fig. 18. Effect of temperature on dehydration conversion and reaction rate for a water vapor pressure of around 1 mbar using a heating rate of 10 [K/min].

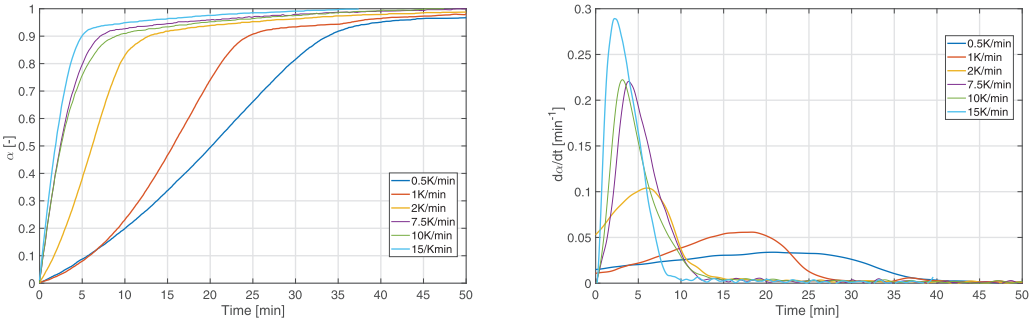

(a) Conversion for various heating rates (b) Reaction rate for various heating rates

Fig. 19. dehydration conversion and reaction rate for various heating rates with a final temperature of 100 °C and an initial sample mass of 10*mg*.

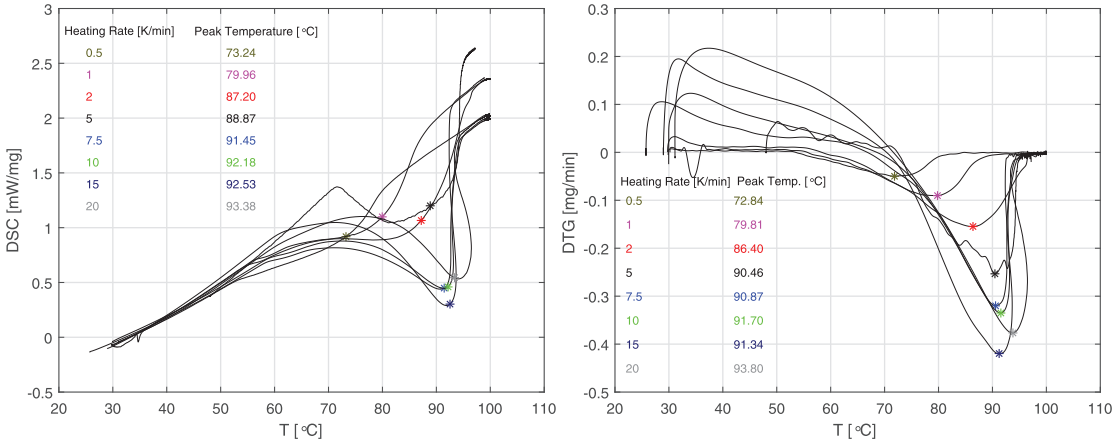

(a) DSC signals versus temperature (b) DTG signals versus temperature

Fig. 20. Peak temperature estimation for dehydration using various heating rates.

Based on so-called Kissinger method, a plot between $ln(\beta/T_{max}^2)$ vs. $(1/T_{max})$ is made, as seen in Fig. 21. The method is based on the Eq. (14), where β[K/min] is the heating rate and $T_{max}[K]$ is the maximum peak temperature. The drawback of this method is that it gives only one set of kinetic parameters, which means one value for Activation energy and exponential pre-factor for whole range of conversion. This could possibly lead to over predicting E_a values. Table 5 shows the values of activation energy

Table 5
Kinetic parameters obtained using Kissinger Method.

	$E_{a,dehyd}$ [kJ/mol]	$A_{f,dehyd}$ [1/min]
Dehydration	78.30563	8.8980×10^{10}

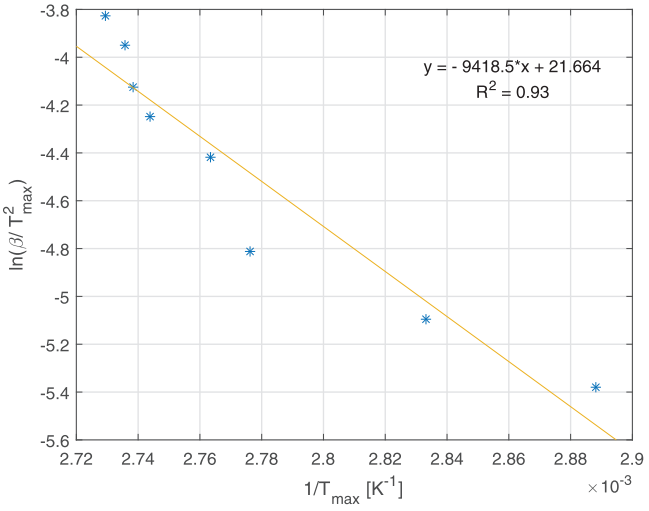

Fig. 21. Kissinger method plot indicating the slope equation and R^2 value.

Table 6
R^2, Goodness of fit coefficient for the numerically obtained α values compared to experimental α values for all heating rates.

β[K/min]	R^2
0.5	0.98
1	0.97
2	0.96
7.5	0.94
10	0.90
15	0.93

and exponential pre-factor calculated based on the Kissinger method.

$$ln\left(\frac{\beta}{T_{max}{}^2}\right) = ln\left(\frac{A_f R}{E_a}\right) - \left(\frac{E_a}{RT_{max}}\right) \quad (14)$$

3.5.5. Final dehydration reaction model

Using Eq. (15) with the kinetics parameters in Table 5, the experimental results can be estimated for dehydration of K_2CO_3.

$$\frac{d\alpha}{dt} = A_f \cdot exp\left(-\frac{E_a}{RT(t)}\right) \cdot (1-\alpha)^{2/3} \cdot \left(\frac{P_{eq}}{P_w}\right) \quad (15)$$

Fig. 22 shows the results of the kinetic model compared to the experimental data for the dehydration of K_2CO_3 using a heating rate of 15 [K/min] from 30 to 100 °C. It is an acceptable fit, however, the conversion is different towards the end. This is due to the thermal lag in the temperature program. Fig. 23 shows the lag in an experimentally measured temperature compared to the programmed temperature. It is not possible to follow the temperature program during the final increase of temperature between 90–100 °C.

To conclude, Fig. 24(a) and (b) show the numerically modelled reaction rates and extent of conversion for different heating rates from 30 to 100 °C using Eq. (15). Table 6 shows the corresponding R^2 values for the model fits with experimental data for determining the accuracies of the fits. The values are close to 1 indicating the model to be a good fit compared with the experimental results, except for higher heating rates, which can be explained due to the thermal lag in the temperature profiles.

3.6. Enthalpy of reaction

This section presents the results of experiments performed to find the enthalpy of reaction calculated using DSC signals, for both dehydration and hydration. The values of energy storage density, energy stored/released and peak power is determined based on the hydration isotherm and heating rate for the hydration and dehydration processes, respectively. The setup can log the TG and DSC signals simultaneously, which allows to estimate the thermal energy change per mole of H_2O. The principle of determining the released heat during hydration or dehydration of a sample is explained in Section 2.4.

Table 7
Specific reaction enthalpy, energy storage density per unit of mass and unit of volume, based on the experiment presented in Fig. 25.

β [K/min]	Δh [kJ/mol]	Δh [MJ/kg]	E/V [GJ/m^3]
10	64.01	0.71	1.27

Fig. 25 shows the DSC signal and loading vs. time for a 8 mg sample, which was dehydrated with a heating rate of 10 [K/min]. It can be seen that the state of hydration is anhydrous after the dehydration process is finished. Correspondingly, a DSC peak can be seen, which is integrated to obtain the stored heat during the endothermic reaction of dehydration. The interval for integration is the time in which the loss of water molecules starts until the sample is anhydrous. The area under the peak is obtained through integration. Fig. 25(a) indicates the energy stored in [mJ] and the peak power in [mW]. Using the obtained values, the specific reaction enthalpy (per mole of water), energy storage density per unit of mass (of dry salt) and volume (of the crystal of the salt) are calculated and presented in Table 7.

A similar analysis is done for hydration of K_2CO_3 using the same principle as used for dehydration. The released heat during hydration of K_2CO_3 between an- and sesquihydrate state for various hydration isotherm temperatures is shown in Fig. 26.

Fig. 26(a) shows the DSC data for hydration of a 8 mg K_2CO_3 sample for varying temperatures using a water vapor pressure of 13 mbar. The energy released in [mJ] and the maximum released power in [mW] are also indicated. The energy released obtained through integration is the area under the peak above the zero baseline, which is the horizontal axis for all signals. The maximum released power is the power released once the hydration is initiated, which keeps decreasing as the reaction progresses. Fig. 26(b) shows the corresponding loading calculated based on the TG signal.

It can be observed that even though the maximum released power values decrease with increase in temperature, the area under the peaks is more or less the same, between 4700 – 4800 [mJ]. Fig. 11 shows the results of reaction rates for the same set of experiments. It can be seen that, the reaction rates directly translates to maximum power released. Higher the reaction rate, higher is the maximum power released for varying isotherm temperature.

As the dependence of maximum power released on various temperature is observed, a similar dependence can be observed between maximum power released and different values of the applied water vapor pressure. However, dependence of water vapor pressure on power released for K_2CO_3 is not considered in this study. Such dependencies between peak power and water vapor pressure have been observed with the use of salt hydrates like calcium chloride and magnesium chloride [20].

The experimental values of specific reaction enthalpy and energy densities for hydration of K_2CO_3 are presented in Table 8. Based on NBS tables [36], the literature value for specific enthalpy is 65.4 [kJ/mol]. The experimental values for enthalpy are lower than the theoretical value by 6 – 7%.

So far, the energy storage density values that have been calculated are based on the crystal density. However, bulk energy stor-

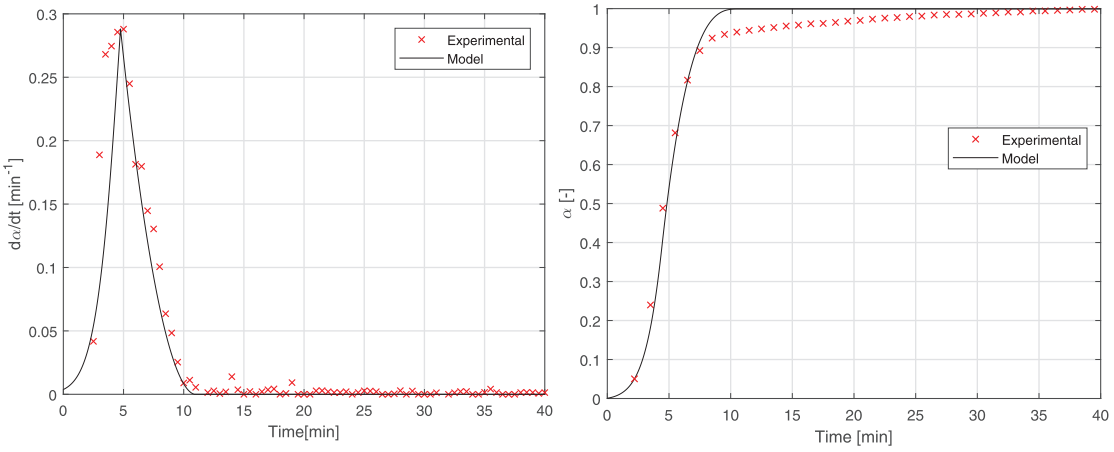

(a) Reaction Rate (b) Conversion

Fig. 22. Comparison between experimental data and numerical kinetic model data for dehydration using a heating rate of 15 [K/min] from 30 to 100 °C.

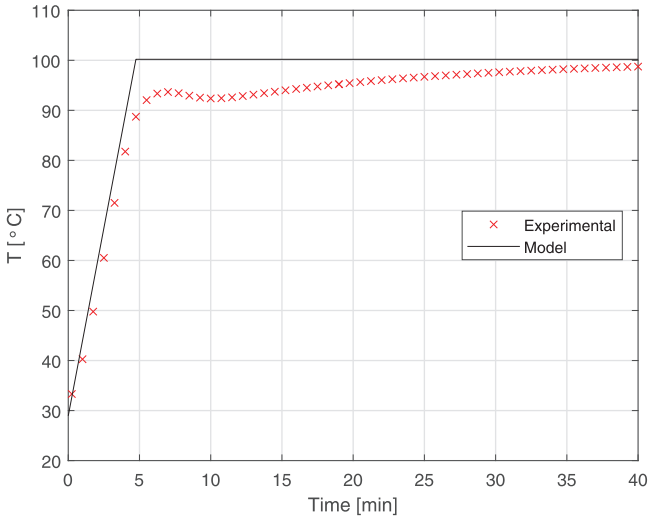

Fig. 23. Modelled temperature profile versus experimental temperature profile of 15 [K/min].

age density can be calculated based on the porosity of the salt hydrate. For a porosity of around 40%, the bulk energy storage density can be calculated to be around 0.75 [GJ/m^3].

Table 8
Specific reaction enthalpy, energy storage density per unit of mass and unit of volume for various hydration isotherms using a water vapor pressure of 13 mbar.

T_{iso} [K/min]	Δh [kJ/mol]	Δh [MJ/kg]	E/V [GJ/m^3]
26	61.54	0.67	1.22
30	60.90	0.66	1.20
40	60.22	0.65	1.19
48	60.87	0.66	1.20

4. Performance in view of application

Based on the developed kinetics and measured enthalpy of reaction, the thermal power of the reaction can be calculated for different conditions. Fig. 27 shows hydration reaction rate vs. extend of conversion at 20 °C hydration isotherm temperature using a water vapor pressure of 13 mbar. As can be seen the maximum reaction rate occurs at the beginning of the process when $\alpha = 0$. Therefore, the maximum power is also achieved at the beginning of the process.

As discussed, the hydration reaction rate varies with temperature in two ways: first, the kinetics constant follows an Arrhenius type of temperature dependency, and second, the equilibrium vapor pressure is dependent on temperature. In Eq. (4), the former

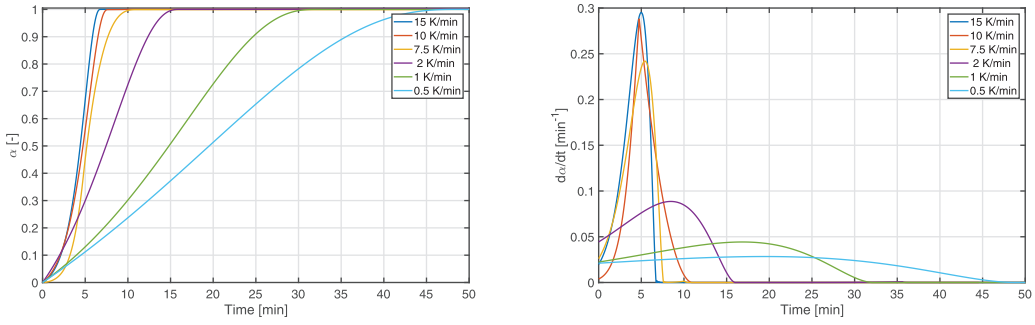

(a) Reaction Rate (b) Conversion

Fig. 24. Numerically modeled reaction rates and extent of conversions for dehydration using various heating rates from 30 to 100 °C.

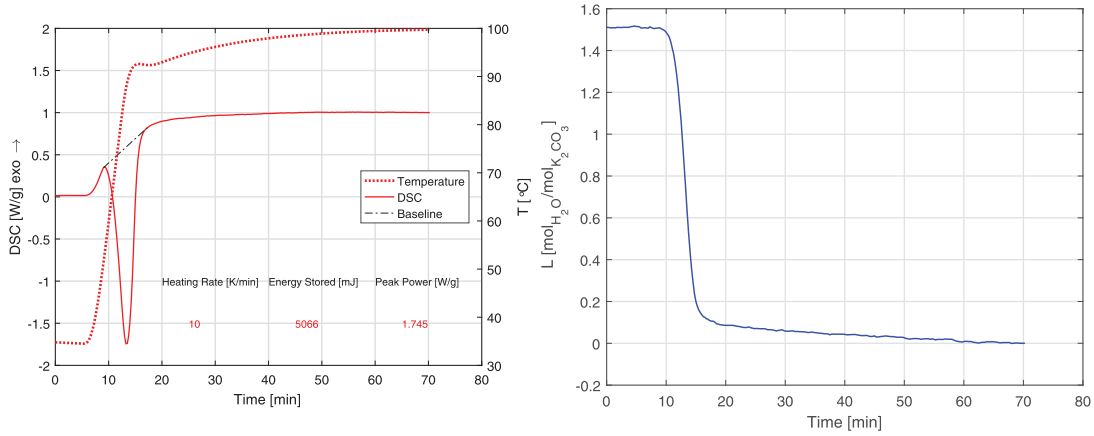

(a) DSC and temperature (b) Loading

Fig. 25. Dehydration of a 8 mg K_2CO_3 sample using a heating rate of 10 [K/min].

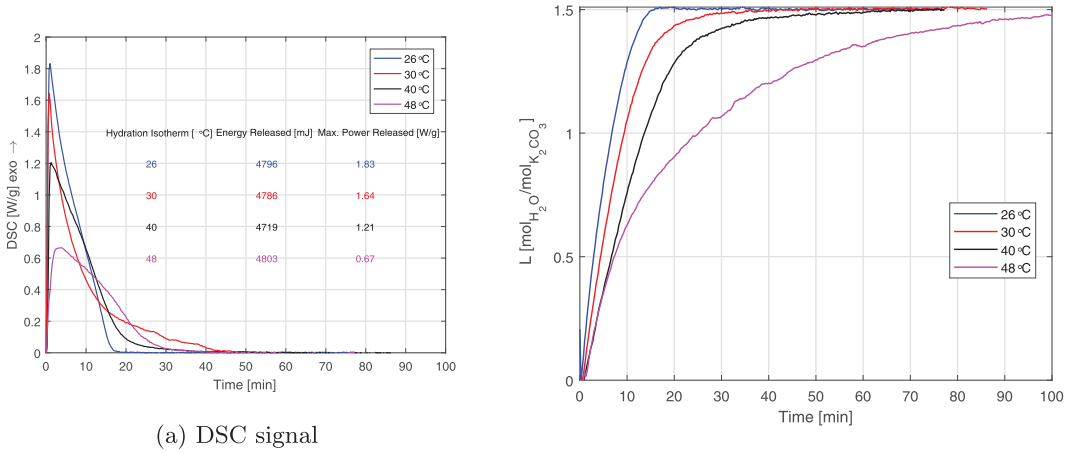

(a) DSC signal (b) Loading

Fig. 26. Hydration of a 8*mg* K_2CO_3 sample using various hydration isotherm temperatures using a water vapor pressure of 13 mbar.

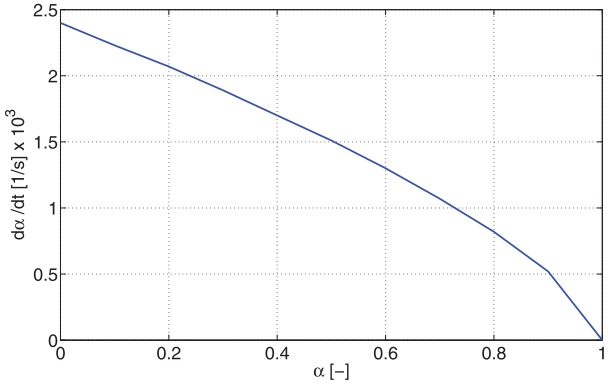

Fig. 27. Reaction rate vs. extend of conversion at 20 °C hydration isotherm temperature using a water vapor pressure of 13 mbar.

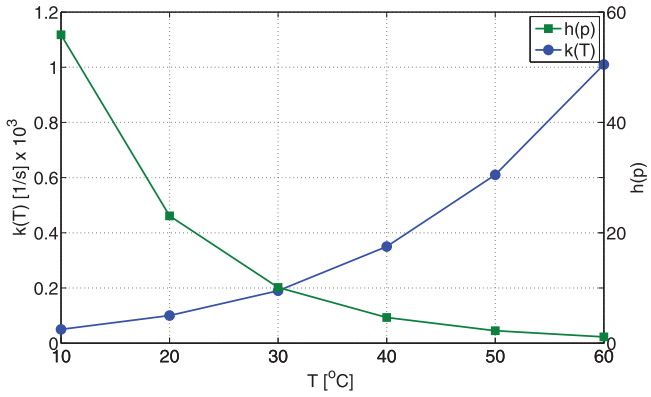

Fig. 28. Temperature and pressure functions for various hydration isotherm temperatures using a water vapor pressure of 13 mbar.

dependency is considered in the kinetics constant $k(T)$ and the latter one in pressure ratio $h(p)$. Fig. 28 shows temperature and pressure functions of reaction rate at its maximum for different temperatures. As can be seen, $k(T)$ increases with temperature, while $h(p)$ decreases.

Fig. 29 shows the maximum rate and thermal power of the hydration reaction. As can be seen, the twofold effect of increasing the temperature leads overall to a decrease in the rate, and hence, in the power. On the other hand, it can be concluded that even though the thermal output is lower at higher temperature, it is still high enough for domestic purposes. For instance at 60 °C, thermal power is around 0.77 W/g at its maximum and more than 0.5 W/g on average.

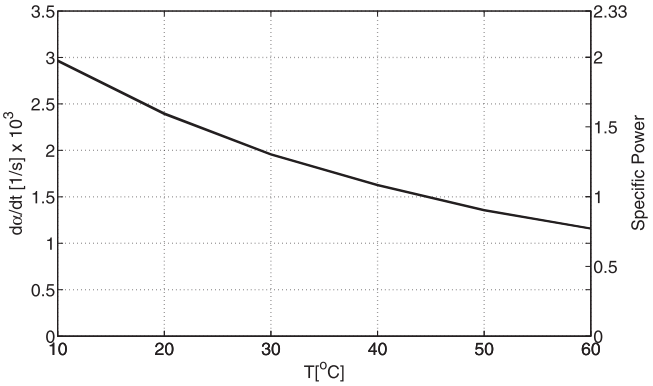

Fig. 29. Maximum reaction rete and power for various hydration isotherm temperatures using a water vapor pressure of 13 mbar.

5. Conclusions

Potassium carbonate, as one of the most promising material for thermochemical heat storage, is investigated in depth on cyclability, kinetics and energy density. In general, a strong relation between conversion rate and sample mass is observed, especially for samples with large masses. This suggests that the hydration reaction of potassium carbonate is a diffusion-limited process. A sample mass of around 10 mg is suggested based on experiments to minimize the effect.

The performance of potassium carbonate improves upon cycling, its kinetics becomes faster after each cycle, up to a certain number of cycles (around 10 cycles) after which it stabilizes. The expansion of the material occurring during each hydration, because of placement of water molecules in the crystal structure, leads to an increase in porosity, and hence, enhanced vapor transport through pores, which results in a faster kinetics.

Kinetics of potassium carbonate hydration and dehydration reactions are studied in different conditions. Hydration and dehydration reaction rates are, respectively, directly and reversely proportional to vapor pressure. Dependency on temperature is twofold: first, in the form of an Arrhenius function for the reaction rate constant; second, in the form of the equilibrium water vapor pressure, which is temperature dependent. The parameters of the Arrhenius functions (pre-exponential constant and activation energy) are extracted for both hydration and dehydration reactions. The reaction order is found to be 2/3 and the reaction model is $f(\alpha) = (1-\alpha)^{2/3}$, which represents a contracting sphere reaction model.

The enthalpy of reaction is calculated to be 64.01 and 60.88 kJ/mol, based on dehydration and hydration experimental results, respectively. The estimated energy density for the bulk material (including bulk porosity) is around 0.75 GJ/m^3.

By increasing temperature, the temperature dependent reaction rate constant $k(T)$ increases, and the pressure dependent function $h(p)$ decreases. The overall rate, and hence, the thermal power of the hydration reaction is lower at higher temperatures. However, the reaction thermal power is high enough for domestic purposes. For instance at 60 °C, thermal power is around 0.77 W/g at its maximum and more than 0.5 W/g on average.

Conflict of interest

None.

Acknowledgements

This research has been made possible by the Energy Pads program, funded by TKIenergo. This work is done in cooperation with Artenergy and De Beijer RTB.

References

[1] Y. Saheb, Modernising Building Energy Codes to Secure our Global Energy Future, 2011.
[2] C. Rindt, S. Lan, M. Gaeini, H. Zhang, S. Nedea, D.M. Smeulders, Phase change materials and thermochemical materials for large-scale energy storage, in: Continuous Media with Microstructure 2, Springer, 2016, pp. 187–197.
[3] J. Jänchen, D. Ackermann, H. Stach, W. Brsicke, Studies of the water adsorption on zeolites and modified mesoporous materials for seasonal storage of solar heat, Solar Energy 76 (13) (2004) 339–344. Solar World Congress 2001. doi: 10.1016/j.solener.2003.07.036.
[4] K.E. NTsoukpoe, T. Schmidt, H.U. Rammelberg, B.A. Watts, W.K. Ruck, A systematic multi-step screening of numerous salt hydrates for low temperature thermochemical energy storage, Appl. Energy 124 (2014) 1–16.
[5] P. Donkers, L. Sögütoglu, H. Huinink, H. Fischer, O. Adan, A review of salt hydrates for seasonal heat storage in domestic applications, Appl. Energy 199 (2017) 45–68.
[6] C. Barreneche, A.I. Fernández, L.F. Cabeza, R. Cuypers, Thermophysical characterization and thermal cycling stability of two tcm: cacl 2 and zeolite, Appl. Energy 137 (2015) 726–730.
[7] C. Bales, P. Gantenbein, D. Jaenig, H. Kerskes, K. Summer, M. van Essen, R. Weber, Laboratory Tests of Chemical Reactions and Prototype Sorption Storage Units, A Report of IEA Solar Heating and Cooling programme-Task, 32, 2008.
[8] M. Gaeini, R. Javed, H. Ouwerkerk, H.A. Zondag, C.C. Rindt, Realization of a 4kw thermochemical segmented reactor in household scale for seasonal heat storage, in: Energy Procedia special issue for 11th International Renewable Energy Storage Conference, IRES 2017, 2017.
[9] K. Johannes, F. Kuznik, J.-L. Hubert, F. Durier, C. Obrecht, Design and characterisation of a high powered energy dense zeolite thermal energy storage system for buildings, Appl. Energy 159 (2015) 80–86.
[10] H. Zondag, B. Kikkert, S. Smeding, R. de Boer, M. Bakker, Prototype thermochemical heat storage with open reactor system, Appl. Energy 109 (2013) 360–365, doi:10.1016/j.apenergy.2013.01.082. http://www.sciencedirect.com/science/article/pii/S0306261913001013.
[11] B. Michel, N. Mazet, P. Neveu, Experimental investigation of an innovative thermochemical process operating with a hydrate salt and moist air for thermal storage of solar energy: global performance, Appl. Energy 129 (2014) 177–186, doi:10.1016/j.apenergy.2014.04.073. http://www.sciencedirect.com/science/article/pii/S030626191400436X.
[12] A. Solé, I. Martorell, L.F. Cabeza, State of the art on gas–solid thermochemical energy storage systems and reactors for building applications, Renew. Sustain. Energy Rev. 47 (2015) 386–398.
[13] L. Scapino, H.A. Zondag, J. Van Bael, J. Diriken, C.C. Rindt, Sorption heat storage for long-term low-temperature applications: a review on the advancements at material and prototype scale, Appl. Energy 190 (2017) 920–948.
[14] L. Scapino, H. Zondag, J. Van Bael, J. Diriken, C. Rindt, Energy density and storage capacity cost comparison of conceptual solid and liquid sorption seasonal heat storage systems for low-temperature space heating, Renew. Sustain. Energy Rev. 76 (2017) 1314–1331. Cited By 0 doi: 10.1016/j.rser.2017.03.101.
[15] P. Donkers, S. Beckert, L. Pel, F. Stallmach, M. Steiger, O. Adan, Water transport in $MgSo_4 7H_2O$ during dehydration in view of thermal storage, J. Phys. Chem. C 119 (52) (2015) 28711–28720. Cited By 5. doi: 10.1021/acs.jpcc.5b08730.
[16] K. Posern, C. Kaps, Humidity controlled calorimetric investigation of the hydration of $MgSo_4$ hydrates, J. Thermal Anal. Calorim. 92 (3) (2008) 905–909. Cited By 26. doi: 10.1007/s10973-007-8640-4.
[17] K. Posern, C. Kaps, Calorimetric studies of thermochemical heat storage materials based on mixtures of $MgSo_4$ and $MgCl_2$, Thermochimica Acta 502 (1–2) (2010) 73–76. Cited By 44. doi: 10.1016/j.tca.2010.02.009.
[18] V. Van Essen, H. Zondag, J. Cot Gores, L. Bleijendaal, M. Bakker, R. Schuitema, W. Van Helden, Z. He, C. Rindt, Characterization of $MgSo_4$ hydrate for thermochemical seasonal heat storage, J. Solar Energy Eng. Trans. ASME 131 (4) (2009) 0410141–0410147. Cited By 56. doi: 10.1115/1.4000275.
[19] C.J. Ferchaud, H.A. Zondag, J.B.J. Veldhuis, R. de Boer, Study of the reversible water vapour sorption process of $MgSo_4$.7h 2 o and $MgCl_2$.6h 2 o under the conditions of seasonal solar heat storage, J. Phys. 395 (1) (2012) 012069. http://stacks.iop.org/1742-6596/395/i=1/a=012069
[20] H.U. Rammelberg, T. Schmidt, W. Ruck, Hydration and dehydration of salt hydrates and hydroxides for thermal energy storage - kinetics and energy release, Energy Procedia 30 (2012) 362–369, doi:10.1016/j.egypro.2012.11.043.
[21] B. Michel, N. Mazet, S. Mauran, D. Stitou, J. Xu, Thermochemical process for seasonal storage of solar energy: characterization and modeling of a high density reactive bed, Energy 47 (1) (2012) 553–563. Cited By 60. doi: 10.1016/j.energy.2012.09.029.
[22] M. Molenda, J. Stengler, M. Linder, A. Wrner, Reversible hydration behavior of $CaCl_2$ at high H_2Opartial pressures for thermochemical energy storage, Thermochimica Acta 560 (2013) 76–81. Cited By 21. doi: 10.1016/j.tca.2013.03.020.
[23] M. Gaeini, A. Rouws, J. Salari, H. Zondag, C. Rindt, Characterization of microencapsulated and impregnated porous host materials based on calcium chloride for thermochemical energy storage, Appl. Energy 212 (2018) 1165–1177. Cited By 0. doi: 10.1016/j.apenergy.2017.12.131.
[24] L. Sögütoglu, P. Donkers, H. Fischer, H. Huinink, O. Adan, In-depth investigation of thermochemical performance in a heat battery: cyclic analysis of K_2CO_3, $MgCl_2$ and Na_2S, Appl. Energy 215 (2018) 159–173. Cited By 0. doi: 10.1016/j.apenergy.2018.01.083.

[25] M. Gaeini, R. van Alebeek, L. Scapino, H. Zondag, C. Rindt, Hot tap water production by a 4kw sorption segmented reactor in household scale for seasonal heat storage, J. Energy Storage 17 (2018) 118–128. Cited By 0. doi: 10.1016/j.est.2018.02.014.
[26] A.F. Lele, F. Kuznik, H.U. Rammelberg, T. Schmidt, W.K. Ruck, Thermal decomposition kinetic of salt hydrates for heat storage systems, Appl. Energy 154 (2015) 447–458.
[27] S. Vyazovkin, A.K. Burnham, J.M. Criado, L.A. Pérez-Maqueda, C. Popescu, N. Sbirrazzuoli, ICTAC Kinetics committee recommendations for performing kinetic computations on thermal analysis data, Thermochimica Acta 520 (1–2) (2011) 1–19, doi:10.1016/j.tca.2011.03.034.
[28] Alibaba.com, http://www.alibaba.com/l.
[29] L. Greenspan, Humidity fixed points of binary saturated aqueous solutions, J. Res. Natl. Bur.Stand. -A 81 (1) (1976). http://nvlpubs.nist.gov/nistpubs/jres/81A/jresv81An1p89_A1b.pdf
[30] M.A. Stanish, D.D. Perlmutter, Kinetics and transport effects in the dehydration of crystalline potassium carbonate hydrate, AIChE J. 29 (5) (1983) 806–812, doi:10.1002/aic.690290515.
[31] M.A. Stanish, D.D. Perlmutter, Rate processes in cycling a reversible gas solid reaction, AIChE J. 30 (1) (1984) 56–62, doi:10.1002/aic.690300110.
[32] L. Glasser, Thermodynamics of inorganic hydration and of humidity control, with an extensive database of salt hydrate pairs, J. Chem. Eng. Data 59 (2) (2014) 526–530, doi:10.1021/je401077x.
[33] E. Washburn, International critical tables of numerical data, physics, chemistry and technology, 1st Electronic ed. Knovel (2003). http://app.knovel.com/hotlink/toc/id:kpICTNDPC4/international-critical/international-critical
[34] M. Lebrun, B. Spinner, Models of heat and mass transfers in solid—gas reactors used as chemical heat pumps, Chem. Eng. Sci. 45 (7) (1990) 1743–1753, doi:10.1016/0009-2509(90)87052-t.
[35] A.F. Lele, A Thermochemical Heat Storage System for Households, Springer-Verlag GmbH, 2016, doi:10.1007/978-3-319-41228-3.
[36] D.D. Wagman, W.H. Evans, V.B. Parker, R.H. Schumm, I. Halow, The NBS tables of chemical thermodynamic properties, Technical Report, DTIC Document, 1982.